NASA TN D-461

TECHNICAL NOTE
D-461

SOME DIVERGENCE CHARACTERISTICS OF LOW-ASPECT-RATIO WINGS AT TRANSONIC AND SUPERSONIC SPEEDS

By Donald S. Woolston, Frederick W. Gibson, and Herbert J. Cunningham

Langley Research Center
Langley Field, Va.

NATIONAL AERONAUTICS AND SPACE ADMINISTRATION
WASHINGTON
September 1960

X

NATIONAL AERONAUTICS AND SPACE ADMINISTRATION

TECHNICAL NOTE D-461

SOME DIVERGENCE CHARACTERISTICS OF LOW-ASPECT-RATIO WINGS AT TRANSONIC AND SUPERSONIC SPEEDS

By Donald S. Woolston, Frederick W. Gibson, and
Herbert J. Cunningham

SUMMARY

The problem of chordwise, or camber, divergence at transonic and supersonic speeds is treated with primary emphasis on slender delta wings having a cantilever support at the trailing edge. Experimental and analytical results are presented for four wing models having apex half-angles of 5°, 10°, 15°, and 20°. A Mach number range from 0.8 to 7.3 is covered.

The analytical results include calculations based on small-aspect-ratio theory, lifting-surface theory, and strip theory. A closed-form solution of the equilibrium equation is given, which is based on low-aspect-ratio theory but which applies only to certain stiffness distributions. Also presented is an iterative procedure for use with other aerodynamic theories and with arbitrary stiffness distribution.

INTRODUCTION

The current trend toward the use of thin, low-aspect-ratio, all-movable control surfaces on aircraft and missiles has introduced the possibility that divergence rather than flutter may be the primary aeroelastic problem for such surfaces. This possibility results from the fact that on all-movable surfaces the forward portion of the surface may be supported from the rear rather than from the side. The resulting chordwise divergence is characterized by a camber type of deformation rather than a twisting or torsion of the wing span. The present paper considers the problem of chordwise divergence at transonic and supersonic speeds and is principally concerned with the divergence of slender delta wings having a cantilever support at the trailing edge.

The problem of chordwise bending in two-dimensional supersonic flow has been treated by Biot (refs. 1 and 2) and by Miles, according to reference 3. The three-dimensional case has also been examined by Miles (ref. 3) and in the more recent investigations of references 4

and 5. The chordwise divergence of an all-movable control at transonic and supersonic speeds has been treated in reference 6.

The purpose of the present paper is to give the results of a reexamination and extension of the material presented in reference 5 which had only limited distribution. The authors of this paper, who collaborated in preparing the results of reference 5, have obtained additional results on the basis of lifting-surface theory for supersonic flow. The investigation includes the development of an iterative solution to the equilibrium equation applicable to divergence studies of configurations with arbitrary stiffness distribution and, also, a closed-form solution applicable to certain special distributions of stiffness. Experimental results are presented for a series of cantilever delta wings having apex half-angles of 5°, 10°, 15°, and 20° over a Mach number range from 0.8 to 7.3. Comparative divergence calculations for these cases based on small-aspect-ratio theory, lifting-surface theory, and strip theory are made.

SYMBOLS

A_{ij}	curvature influence coefficient, $(\text{ft-lb})^{-1}$ (eqs. (30))
a_{nm}	weighting factor in series form of $\Delta p(x,y)$ (eq. (3))
B_{ij}	slope influence coefficient, lb^{-1}, (eqs. (37))
$[B_1]$	matrix defined by equation (42), ft^2
$[B_2]$	matrix defined by equation (46), ft
C_β	torsional spring constant, ft-lb/radian
c_0	chord at wing plane of symmetry, ft
$[D]$	differentiating matrix, ft^{-1} (see eq. (44))
E, E(x)	modulus of elasticity, lb/sq ft
F(x)	local aerodynamic force per unit span, lb/ft
F_j	concentrated aerodynamic load at x_j, lb
h	local vertical displacement, ft

$I(x)$ section moment of inertia, ft^4

$[I_1]$ integrating matrix, ft (see eq. (32))

J_ν, J_μ Bessel function of the first kind of order ν and μ, respectively

K, $K(M,k,x-x',y-y')$ kernel function of integral equation, ft^{-2}

K_0 section moment of inertia constant (eq. (16))

K_1, K_2 divergence constants, defined by equations (25) and (48), respectively

k reduced frequency

k_1 weight constant (see eq. (52))

L_{nm}, $L_{nm}(x,y)$ lift function in series form of $\Delta p(x,y)$ (eq. (3))

M Mach number

$M_B(x)$ local bending moment, ft-lb

q dynamic pressure, $\rho V^2/2$, lb/sq ft

q_d dynamic pressure at divergence, lb/sq ft

S_j area of jth wing segment, sq ft

s local wing half-span, $x \tan \epsilon$, ft

t local thickness, ft

t_0 thickness at midspan of trailing edge, ft

V velocity, fps

W wing weight, lb

x,y,z,x',y' Cartesian coordinates, ft (see fig. 1)

x_i,x_j chordwise coordinates of centers of ith and jth segments, ft

$x_p = c_0 \xi_p$

$\beta = \sqrt{M^2 - 1}$

$\Delta p(x,y)$, $\Delta p(x',y')$ local pressure difference, lb/sq ft

Δx chord of wing segment, ft

ϵ apex half-angle (see fig. 1)

θ angular spanwise variable defined by equation (14)

λ characteristic parameter (see eq. (20))

$\mu = 3/(3-n)$

$\nu = n/(3-n)$

ξ dimensionless chordwise variable, x/c_0

ξ_j dimensionless chordwise coordinate of midpoint of jth segment, x_j/c_0

ξ_p dimensionless chordwise coordinate of wing support station

II_{LK} definite integrals in the lifting-surface-theory problem (see eq. (4))

$II_{nm}^{(j)}$ integrals defined by equation (8), ft^2

ρ fluid density, slugs/cu ft

$\bar{\rho}$ material density, lb/cu ft

Superscripts:

n, m denote powers of the chordwise and spanwise variables, respectively, in the expression for the thickness distribution (see eq. (12))

Matrix notation:

$[\ ]$ square matrix

$\lfloor\ \rfloor$ row matrix

$\{\ \}$ column matrix

$[\ ]$ diagonal matrix

FORMULATION OF THE PROBLEM

The Equilibrium Equation

The problem at hand is that of the divergence of a delta-wing planform, shown in figure 1, which is restrained along a section normal to its root chord at some distance x_p from its apex. The wing is considered to be capable only of chordwise bending - that is, bending of the mean camber line. The effect of spanwise variation of bending would be expected to be small for the narrow models with the thickness distributions studied herein. The wing in its neutral position is assumed to lie nearly in the xy-plane of an x,y,z coordinate system which moves with the planform in the negative x-direction at uniform velocity V. It is assumed that the wing, so restrained, will obey the mechanics of a simple beam and that the only external forces acting upon it are aerodynamic forces which arise when it is perturbed from its neutral position. Under these conditions the state of equilibrium may be expressed by the following differential equation:

$$\frac{d^2}{dx^2}\left[E(x)I(x)\ \frac{d^2h}{dx^2}\right] = F(x) \tag{1}$$

where $E(x)$ is the modulus of elasticity, $I(x)$ is the section moment of inertia, h is the vertical displacement of any section from its neutral position, and $F(x)$ is the aerodynamic force acting at station x.

The present study includes several stiffness or thickness distributions, leading to different forms of $I(x)$, and considers various linear aerodynamic theories, from which are obtained different forms of $F(x)$. Some examples are treated in which the thickness distribution is described by simple analytic functions of the chordwise coordinate, but consideration is also given to the possibility of an arbitrary thickness distribution.

When certain analytical expressions are chosen to represent the thickness distribution and are used in combination with the aerodynamic forces given by small-aspect-ratio theory or strip theory, closed-form solutions of the equilibrium equation can be obtained. For other combinations of thickness distribution and aerodynamic forces an iterative procedure is developed. Before discussing the methods of solution, the forms of $F(x)$ and $I(x)$ to be employed are considered.

The Aerodynamic Force $F(x)$

The forms of $F(x)$ to be employed depend on the Mach number range to be dealt with and on the apex angle of the structure. If the wing is very slender and if the Mach lines lie well ahead of the leading edge ($\beta \tan \epsilon \ll 1$), small-aspect-ratio theory may be used. For Mach numbers up to that for which the leading edge becomes supersonic, lifting-surface theory based on kernel-function procedures is available. If the leading edge is supersonic and if spanwise variations of deflections are neglected, the loading based on linear theory is given exactly by strip theory, which for sufficiently high Mach numbers corresponds to first-order piston theory.

In the present calculations, small-aspect-ratio theory and lifting-surface theory are used at subsonic speeds, and small-aspect-ratio theory, lifting-surface theory, and strip theory are used at supersonic speeds. Both small-aspect-ratio theory and strip theory are used for comparison throughout the range of supersonic Mach numbers considered even though the Mach number range in which the theories are valid is exceeded.

Small-aspect-ratio theory.- An expression for the aerodynamic force given by small-aspect-ratio theory for the case of steady flow can be obtained directly from the work of Jones (ref. 7) or from Garrick's results for unsteady flow (ref. 8). The force can be expressed in the following form:

$$F(x) = -2\rho V^2 \int_{-x \tan \epsilon}^{x \tan \epsilon} \left(\frac{d^2h}{dx^2} \sqrt{x^2 \tan^2 \epsilon - y^2} + \frac{dh}{dx} \frac{x \tan^2 \epsilon}{\sqrt{x^2 \tan^2 \epsilon - y^2}} \right) dy$$

or

$$F(x) = -2\pi q \tan^2 \epsilon \frac{d}{dx} \left(x^2 \frac{dh}{dx} \right) \qquad (2)$$

where

$$q = \frac{1}{2}\rho V^2$$

Lifting-surface theory.- In order to obtain an expression for the force $F(x)$ based on lifting-surface theory, it is necessary to determine first the chordwise and spanwise distribution of pressure acting on the surface. For this purpose use is made of an integral equation which, in steady flow, relates the slope of the wing surface to the pressure distribution.

The integral equation can be written as

$$\frac{dh}{dx} = \frac{1}{4\pi\rho V^2} \iint_A \Delta p(x',y')K(M,k,x-x',y-y')dx'\,dy'$$

where $K(M,k,x-x',y-y')$ is the kernel function. The quantity $K/4\pi\rho V^2$ is the mathematical expression for the downwash induced at any point x,y by a unit force acting at any other point x',y'. The area A over which the integration extends is the portion of the wing in which a pressure pulse must occur in order to induce vertical velocity at the specified point x,y. In subsonic flow A corresponds to the entire wing surface; in supersonic flow A is that portion of the surface bounded by the planform edges and the forward Mach cone from the point x,y. A numerical method of solving the integral equation for the subsonic case is described in reference 9; the procedure for the supersonic case is based on similar techniques but involves differences in the form of the pressure distribution and in the kernel of the integral equation.

An approximate solution to the integral equation involves expressing the unknown pressure distribution as a sum of chosen modes of lift functions L_{nm} (of forms appropriate to the planform and Mach number range under consideration), each weighted by a constant coefficient to be determined. The following expression is employed:

$$\Delta p(x,y) = 8\pi q\left[L_{nm}\right]\left\{a_{nm}\right\} \tag{3}$$

Through the use of this expression the integral equation can be represented as a summation of definite integrals and can be solved by numerical methods. The following matrix form of the integral equation can then be written:

$$\left\{\frac{dh}{dx}\right\} = \left[II_{LK}\right]\left\{a_{nm}\right\} \tag{4}$$

where the elements of II_{LK} represent the definite surface integrals of the products of the functions L_{nm} and the kernel function K and the elements $\frac{dh}{dx}$ represent the wing slope at a number of selected points on the wing surface. Equation (4) may therefore be regarded as a set of simultaneous equations from which the values of the weighting factors a_{nm} can be obtained once the definite integrals have been evaluated. (The evaluation of these integrals constitutes the major task in the kernel-function procedure and is accomplished by use of the methods and the computing program described in reference 9; it is not pertinent to the present discussion, however, and need not be considered herein.)

A premultiplication of each side of equation (4) by the inverse matrix $\left[II_{LK}\right]^{-1}$ gives the expression

$$\left[a_{nm}\right] = \left[II_{LK}\right]^{-1}\left\{\frac{dh}{dx}\right\} \tag{5}$$

which can be used to obtain values of the weighting factors a_{nm} for any prescribed slope distribution. Once these weighting factors a_{nm} have been determined, the pressure $\Delta p(x,y)$ associated with the prescribed slope distribution is defined by equation (3).

For use in the influence-coefficient procedures to be described subsequently, it will be necessary to obtain the forces acting on each of the several segments (fig. 2) into which the wing is divided; this will require an integration of the pressure distribution over each segment. The force on the jth segment F_j may be expressed as

$$F_j = \iint_{S_j} \Delta p(x,y)\,dx\,dy \tag{6}$$

or, applying equation (3),

$$F_j = 8\pi q\left[II_{nm}^{(j)}\right]\left\{a_{nm}\right\} \tag{7}$$

where

$$II_{nm}^{(j)} = \iint_{S_j} L_{nm}(x,y)\,dx\,dy \tag{8}$$

and where S_j denotes the area of the jth segment.

Strip theory.- If the leading edge is supersonic and if there is no spanwise variation of wing deflection h, the aerodynamic loading is given exactly (within the limitations of linear theory) by strip theory. (See, for example, refs. 10 and 11.) The force $F(x)$ for use in equation (1) is expressed as

$$F(x) = -\frac{2\rho V^2}{\beta} \int_{-x \tan \epsilon}^{x \tan \epsilon} \frac{dh}{dx}\, dy$$

or

$$F(x) = -\frac{8q}{\beta}\, x \tan \epsilon \frac{dh}{dx} \tag{9}$$

If $M \gg 1$, $F(x)$ can be expressed approximately as

$$F(x) = -\frac{8q}{M}\, x \tan \epsilon \frac{dh}{dx} \tag{10}$$

which is the result given by piston theory (ref. 12) for the case of zero thickness.

Area Moment of Inertia $I(x)$

The term $I(x)$ in equation (1) is the section area moment of inertia and is therefore directly related to the thickness by the expression

$$I(x) = \int_{-x \tan \epsilon}^{x \tan \epsilon} dy \int_{-t/2}^{t/2} z^2 dz = \frac{1}{12} \int_{-x \tan \epsilon}^{x \tan \epsilon} t^3 dy \tag{11}$$

where ϵ is the apex half-angle.

As noted previously, it has been found that, when certain forms of the thickness distribution are used in combination with aerodynamic forces based on small-aspect-ratio theory or strip theory, closed-form solutions of the equilibrium equation are possible. A fairly general form of the thickness distribution which leads to an exact solution is the following expression:

$$t = t_0\left(\frac{x}{c_0}\right)^{n/3}\left(1 - \frac{y^2}{s^2}\right)^{m/12} \tag{12}$$

where t_0 is the thickness at the point $x=c_0, y=0$ and where m and n are positive integers. This expression for t contains a chordwise variation of thickness given by the term in $\frac{x}{c_0}$ and a spanwise variation in thickness given by the term involving $\frac{y}{s}$. It should be remarked that for $n > 3$ the thickness distribution is characterized by a cusp at the apex so that at the apex the leading edge is infinitely sharp. Such thickness distributions are not considered herein since linear beam theory would not be expected to apply.

In order to proceed toward an expression for the moment of inertia $I(x)$, equation (12) may be substituted into equation (11) to obtain

$$I(x) = \frac{t_0^3}{6}\left(\frac{x}{c_0}\right)^n \int_0^s \left(1 - \frac{y^2}{s^2}\right)^{m/4} dy \tag{13}$$

where $s = x \tan \epsilon$ is the local wing half-span and where symmetry about the center line is assumed. The integral in equation (13) can be expressed conveniently in terms of the gamma function and for this purpose there is introduced the angular variable θ defined as

$$\theta = \sin^{-1}\frac{y}{s} \tag{14}$$

in terms of which equation (13) becomes

$$I(x) = \frac{t_0^3}{6}\left(\frac{x}{c_0}\right)^n x \tan \epsilon \int_0^{\pi/2} (\cos \theta)^{(2+m)/2} d\theta \tag{15}$$

If the integral in equation (15) is denoted by K_0, it may be shown that

$$K_0 = \int_0^{\pi/2} (\cos \theta)^{(2+m)/2} d\theta = \frac{\sqrt{\pi}}{2} \frac{\Gamma\left(\frac{m+4}{4}\right)}{\Gamma\left(\frac{m+6}{4}\right)} \tag{16}$$

where Γ denotes the gamma function. The inertia term $I(x)$ may then be expressed as

$$I(x) = K_0 \frac{t_0^3}{6}\left(\frac{x}{c_0}\right)^n x \tan \epsilon \tag{17}$$

Numerical values of the section moment-of-inertia constant K_0 for several values of m are given in table I. Included with table I are sketches of the sections to which the various values of m pertain.

CLOSED-FORM SOLUTIONS OF THE EQUILIBRIUM EQUATION

Exact solutions of the equilibrium equation can be obtained for a few special choices of the section area moment of inertia $I(x)$ given by equation (17) and for the aerodynamic-force distributions $F(x)$ given by small-aspect-ratio theory or by strip theory. These solutions can be used to assess the accuracy of the more generally applicable iterative procedures to be developed. Before considering these solutions it is convenient to arrive at a nondimensional form of the equilibrium equation by introducing the change of variable

$$x = c_0 \xi$$

so that equation (17) becomes

$$I(c_0\xi) = \frac{c_0^4 K_0}{6}\left(\frac{t_0}{c_0}\right)^3 \xi^{n+1} \tan \epsilon$$

With this expression for $I(c_0\xi)$, equation (1) may be written in the desired nondimensional form as

$$\frac{K_0}{6}\left(\frac{t_0}{c_0}\right)^3 \tan \epsilon \frac{d^2}{d\xi^2}\left[E(c_0\xi)\xi^{n+1}\frac{d^2h}{d\xi^2}\right] = F(c_0\xi) \tag{18}$$

If the expression for $F(c_0\xi)$ given by small-aspect-ratio theory (eq. (2)) is employed and if $E(c_0\xi)$ is taken to be constant, equation (18) can be written as

$$\frac{d^2}{d\xi^2}\left(\xi^{n+1}\frac{d^2h}{d\xi^2}\right) + \lambda^2\frac{d}{d\xi}\left(\xi^2\frac{dh}{d\xi}\right) = 0 \tag{19}$$

where

$$\lambda^2 = \frac{12\pi q \tan\epsilon}{K_0 E\left(\frac{t_0}{c_0}\right)^3} \tag{20}$$

Solutions to equation (19) will be obtained for values of n of 0, 1, 2, and 3 for two types of wing mounting.

First, however, it is noted that a solution of equation (18) can also be obtained, provided $n = 3$, when the aerodynamic-force distribution is given by strip theory (eq. (9)). In this event equation (18) becomes

$$\frac{K_0}{6}\left(\frac{t_0}{c_0}\right)^3 \tan\epsilon\,\frac{d^2}{d\xi^2}\left[E(c_0\xi)\xi^4\frac{d^2h}{d\xi^2}\right] + \frac{8q}{\beta}\xi\tan\epsilon\frac{dh}{d\xi} = 0$$

or taking $E(c_0\xi)$ as a constant and performing the indicated differentiations of the first term results in

$$\xi^4\frac{d^4h}{d\xi^4} + 8\xi^3\frac{d^3h}{d\xi^3} + 12\xi^2\frac{d^2h}{d\xi^2} + \Lambda\xi\frac{dh}{d\xi} = 0$$

in which

$$\Lambda = \frac{48q}{\beta K_0\left(\frac{t_0}{c_0}\right)^3}$$

This form of the equilibrium equation is of the form of Cauchy's equidimensional linear differential equation, the solution of which is discussed, for example, in section 1.6 of reference 13.

Exact Solution for the Trailing-Edge-Cantilevered Delta Wing Based on Small-Aspect-Ratio Theory

In order to complete the formulation of the divergence problem as expressed by equation (19), it is necessary to impose certain conditions at the apex and at the point of support. Conditions to be imposed at the apex imply no bending moment or shear and are

$$\left.\begin{aligned} &\lim_{\xi \to 0} \xi^{n+1} \frac{d^2h}{d\xi^2} = 0 \\ &\lim_{\xi \to 0} \frac{d}{d\xi}\left(\xi^{n+1} \frac{d^2h}{d\xi^2}\right) = 0 \end{aligned}\right\} \tag{21}$$

For the trailing-edge-cantilevered delta wings, the conditions to be imposed imply that there is no displacement or slope at the built in edge and are

$$h_{\xi=1} = \left(\frac{dh}{d\xi}\right)_{\xi=1} = 0 \tag{22}$$

After one integration and the imposition of the apex conditions equation (19) becomes

$$\frac{d}{d\xi}\left(\xi^{n+1} \frac{d^2h}{d\xi^2}\right) + \lambda^2 \xi^2 \frac{dh}{d\xi} = 0$$

or, if $\frac{dh}{d\xi} = f$,

$$\frac{d}{d\xi}\left(\xi^{n+1} \frac{df}{d\xi}\right) + \lambda^2 \xi^2 f = 0$$

This may be recognized as a special form of Bessel's equation. (See, for example, eq. (123e), p. 167, of ref. 13.) If $n \neq 3$, a solution under the apex conditions imposed by equation (21) is found to be

$$h = C_1 \int \xi^{-n/2} J_\nu \left[\frac{2\lambda}{3 - n} \xi^{(3-n)/2} \right] d\xi + C_2 \tag{23}$$

where J_ν is the Bessel function of the first kind of order ν ($\nu = n/(3 - n)$) and C_1 and C_2 are constants. (If $n = 3$, the problem is soluble as an equidimensional equation (sec. 1.6, ref. 13). From equations (22) and (23), the eigenvalues for the cantilevered case ($n \neq 3$) are the roots of

$$J_\nu \left[\frac{2\lambda}{3 - n} (\xi)^{(3-n)/2} \right] = 0 \tag{24}$$

In order to assess the accuracy of the iterative procedures to be discussed subsequently, solutions to the differential equations have been obtained for constant E and for a thickness distribution defined by setting $m = 0$ in equation (12) so that

$$t = t_0 (\xi)^{n/3}$$

and for $n = 0$, 1, 2, and 3. For $n = 0$, 1, and 2 the roots of the Bessel functions in equation (24) and the corresponding values of λ are as follows:

n	$\nu = \frac{n}{3 - n}$	Equation in λ	Root of $J_\nu = 0$	λ
0	0	$J_0\left(\frac{2\lambda}{3}\right) = 0$	2.4048	3.6072
1	1/2	$J_{1/2}(\lambda) = 0$	π	π
2	2	$J_2(2\lambda) = 0$	5.1356	2.5678

For $n = 3$ there is found a corresponding value of λ of 1.499. The quantity λ^2 in equation (19) may be used to form a convenient divergence constant K_1 defined as

$$K_1 = \frac{\lambda^2}{12\pi} = \frac{q_d \tan \epsilon}{E K_0 \left(\frac{t_0}{c_0} \right)^3} \tag{25}$$

Values of K_1 for the foregoing examples are listed in table II.

Exact Solution for the All-Movable Control Based on Small-Aspect-Ratio Theory

An alternative configuration which might be treated is the all-movable control attached to a torque rod at $\xi = \xi_p$ where ξ_p is the chordwise coordinate of the pitch axis and is referred to c_0 as unit length. For this case the conditions to be imposed at the section of support would be

$$\left.\begin{aligned} h(\xi_p) &= 0 \\ M_B(\xi_p) &= C_\beta\left(\frac{dh}{c_0 d\xi}\right)_{\xi_p} \end{aligned}\right\} \tag{26}$$

where

$$M_B(\xi_p) = c_0^2 \int_0^1 (\xi - \xi_p)F(\xi)d\xi$$

or, from equation (2),

$$M_B(\xi_p) = -2\pi q \tan^2\epsilon c_0^2 \int_0^1 (\xi - \xi_p)\frac{d}{d\xi}\left(\xi^2 \frac{dh}{d\xi}\right)d\xi \tag{27}$$

is the total aerodynamic moment about the pitch axis $\xi = \xi_p$ and where C_β represents the torsional spring constant of the torque rod.

In order to obtain an expression for the eigenvalues for the all-movable control attached to a pitch spring, the expression for h given by equation (23) must be substituted into equation (27); after the resulting expression is integrated, the expression which defines the eigenvalues is

$$-\lambda^2 E K_0\left(\frac{t_0}{c_0}\right)^3 \tan\epsilon\left[(1 - \xi_p)J_\nu\left(\frac{2\lambda}{3-n}\right) - \frac{1}{\lambda}J_\mu\left(\frac{2\lambda}{3-n}\right)\right] = 6C_\beta J_\nu\left[\frac{2\lambda}{3-n}(\xi_p)^{(3-n)/2}\right] \tag{28}$$

where $\mu = 3/(3 - n)$ and, as stated previously, $\nu = n/(3 - n)$.

ITERATIVE SOLUTIONS OF THE EQUILIBRIUM EQUATION

The exact solutions of the equilibrium equations which were outlined in the preceding section are applicable only to calculations based on certain aerodynamic-force representations and thickness distributions. For other cases it is necessary to seek an approximate solution; in the present investigation an iterative procedure based on influence coefficients is employed.

No proof of convergence of the iterative procedure is attempted. In the calculations described in reference 5 for the case of an all-movable control with the hinge axis not at the trailing edge, some difficulty with convergence was experienced in a few cases for which the control surface was very stiff and the torque rod was very weak. It was found, however, that by averaging the results of two successive cycles of iteration and employing the average to start the next cycle convergence could be obtained. No such difficulty was encountered in the present calculations for the delta wings with a cantilever support at the trailing edge.

Formulations of the equilibrium equation based both on curvature influence coefficients (eq. (31)) and on slope influence coefficients (eq. (34)) will be given. Either formulation may be used, the choice being dictated by convenience in obtaining the necessary structural and aerodynamic data.

Influence-Coefficient Forms of the Equilibrium Equation

As is the usual practice, the wing is considered to be made up of a finite number of segments (fig. 2). In the calculations for supersonic flow, 10 segments were used and comparisons with exact results (to be discussed in a subsequent section) showed this number of segments to be adequate. In the calculations for subsonic flow, first 10 and then 16 segments were used; the additional segments were added near the apex between 0 and 0.3 chord. The results were not changed by the addition of these segments.

The force acting on each segment is assumed to be concentrated at the midpoint of the segment and the slope or curvature is measured there. The analysis proceeds from the fundamental beam relation between curvature and bending moment, namely,

$$\frac{d^2h}{dx^2} = \frac{M_B(x)}{EI(x)} \tag{29}$$

where $M_B(x)$ is bending moment.

Curvature equation.- For arbitrary distributions of stiffness, equation (29) can be used directly to formulate an iterative procedure based on curvature influence coefficients. If A_{ij} denotes the curvature produced at x_i by a unit load F_j at x_j, there can be obtained from equation (29) the relations

$$A_{ij} = \frac{\left(\frac{d^2h}{dx^2}\right)_{x_i}}{F_j} = \frac{x_i - x_j}{E(x_i)I(x_i)} \qquad (x_i > x_j) \qquad (30a)$$

and

$$A_{ij} = 0 \qquad (x_i \leqq x_j) \qquad (30b)$$

Equations (30) are used to evaluate the curvature influence coefficients A_{ij} and also to provide the following matrix form of the equilibrium equation:

$$\left\{\left(\frac{d^2h}{dx^2}\right)_{x_i}\right\} = \left[A_{ij}\right]\left\{F_j\right\} \qquad (31)$$

The aerodynamic forces F_j acting on the various segments can be expressed as functions of the curvature to obtain a form of the equilibrium equation which may be iterated until convergence upon a curvature distribution is obtained. The manner of doing this for the various aerodynamic theories is indicated in the next section.

Slope equation.- A matrix form of the equilibrium equation based on slope influence coefficients may be obtained directly from equation (31) by the introduction of a suitable integrating matrix $\left[I_1\right]$ which gives the results

$$\left[I_1\right]\left\{\left(\frac{d^2h}{dx^2}\right)_{x_i}\right\} = \left\{\left(\frac{dh}{dx}\right)_{x_i}\right\} \qquad (32)$$

and

$$\left[I_1\right]\left[A_{ij}\right] = \left[B_{ij}\right] \qquad (33)$$

where an element B_{ij} denotes the slope produced at x_i by a unit load at x_j.

A sample integrating matrix appropriate to the 10-segment system and the trailing-edge-cantilevered models treated herein is given in table III. Multiplying both sides of equation (31) by the matrix $[I_1]$ leads to the following expression:

$$\left\{\left(\frac{dh}{dx}\right)_{x_i}\right\} = [I_1][A_{ij}]\{F_j\} = [B_{ij}]\{F_j\} \tag{34}$$

This expression provides the basis for iteration on the slope distribution for a structure with arbitrary stiffness.

For the special cases for which the thickness distribution is specified by equation (12) and for which the material is homogeneous, equation (29) can be integrated in closed form to obtain an analytic expression for the slope influence coefficients B_{ij}. For such cases $I(x)$ is given by equation (17) in terms of the dimensionless variable $\xi = x/c_0$ as

$$I(x) = \frac{K_0 t_0^3}{6} (\xi)^n c_0 \xi \tan \epsilon \tag{35}$$

By substituting this result into equation (30a) the following expression is obtained for the curvature at ξ due to an arbitrary load F_j at ξ_j where $\xi > \xi_j$:

$$\frac{d^2h}{dx^2} = \frac{6F_j}{K_0 E t_0^3 \tan \epsilon} \frac{\xi - \xi_j}{(\xi)^{n+1}} \tag{36}$$

This result can be integrated to obtain the following expressions for B_{ij} for $n = 0$, 1, 2, and 3 and for $\xi_i \geqq \xi_j$:

For $n = 0$,

$$B_{ij} = \frac{\left(\frac{dh}{dx}\right)_{\xi_i}}{F_j} = \frac{6c_0}{K_0 E t_0^3 \tan \epsilon}\left(1 - \xi_i + \xi_j \log \xi_i\right) \tag{37a}$$

$n = 1$,

$$B_{ij} = \frac{6c_0}{K_0 E t_0^3 \tan \epsilon}\left(\xi_j - \log \xi_i - \frac{\xi_j}{\xi_i}\right) \tag{37b}$$

$n = 2$,

$$B_{ij} = \frac{6c_0}{K_0 E t_0^3 \tan \epsilon}\left(-1 + \frac{\xi_j}{2} + \frac{1}{\xi_i} - \frac{\xi_j}{2\xi_i^2}\right) \tag{37c}$$

and $n = 3$,

$$B_{ij} = \frac{6c_0}{K_0 E t_0^3 \tan \epsilon}\left(-\frac{1}{2} + \frac{\xi_j}{3} + \frac{1}{2\xi_i^2} - \frac{\xi_j}{3\xi_i^3}\right) \tag{37d}$$

For $\xi_i < \xi_j$,

$$B_{ij} = B_{jj} \tag{38}$$

Solutions Based on Small-Aspect-Ratio Theory

Equation (2) can be used to express the aerodynamic-force distribution given by small-aspect-ratio theory in terms of slope and curvature as

$$F(x) = -2\pi q \tan^2 \epsilon\left(2x \frac{dh}{dx} + x^2 \frac{d^2h}{dx^2}\right) \tag{39}$$

If the force is evaluated at x_j, the center of the jth segment, and is considered to be constant over the segment, the matrix of aerodynamic forces $\{F_j\}$ for use in the equilibrium equation may be then written as

$$\{F_j\} = -2\pi q\,\Delta x \tan^2\epsilon \left\{ x_j^2 \left(\frac{d^2h}{dx^2}\right)_{x_j} + 2x_j \left(\frac{dh}{dx}\right)_{x_j} \right\} \qquad (40)$$

where Δx is the chord of the (equal) segments.

Curvature equation.- For use in equation (31) it is desired that F_j be expressed as a function of curvature only. For this purpose equations (32) and (40) can be used to write

$$\{F_j\} = -2\pi q\,\Delta x [B_1] \left\{ \left(\frac{d^2h}{dx^2}\right)_{x_j} \right\} \qquad (41)$$

where

$$[B_1] = \tan^2\epsilon \left[[x_j^2] + 2[x_j][I_1] \right] \qquad (42)$$

Substitution of equation (41) into equation (31) yields

$$\left\{ \left(\frac{d^2h}{dx^2}\right)_{x_i} \right\} = -2\pi q\,\Delta x [A_{ij}][B_1] \left\{ \left(\frac{d^2h}{dx^2}\right)_{x_j} \right\} \qquad (43)$$

which may be solved by iteration upon the curvature to obtain the value of dynamic pressure at divergence.

Slope equation.- It is possible to obtain the matrix $\{F_j\}$ of equation (40) in a form which involves only the slope and which can therefore be used with slope influence coefficients in equation (34). For this purpose a differentiating matrix $[D]$ is needed to yield

$$\left\{\frac{d^2h}{dx^2}\right\} = [D]\left\{\frac{dh}{dx}\right\} \tag{44}$$

A suitable differentiating matrix for use with the 10-point system of the present study was obtained in reference 6 and is given in table IV. The use of this differentiating matrix in equation (40) gives

$$\{F_j\} = -2\pi q\,\Delta x[B_2]\left\{\left(\frac{dh}{dx}\right)_{x_j}\right\} \tag{45}$$

where

$$[B_2] = \tan^2\epsilon\left[\left[x_j^2\right][D] + 2\left[x_j\right]\right] \tag{46}$$

Equation (45) may be substituted into equation (34) to obtain the following expression:

$$\left\{\left(\frac{dh}{dx}\right)_{x_i}\right\} = -2\pi q\,\Delta x[B_{ij}][B_2]\left\{\left(\frac{dh}{dx}\right)_{x_j}\right\} \tag{47}$$

which may be solved by iteration upon the slope to obtain the value of dynamic pressure at divergence.

Numerical results.- In order to help determine the accuracy of the iterative procedure, solutions to equations (43) and (47) have been obtained for the thickness distributions for which closed-form solutions were obtained.

Values of the divergence parameter K_1, equation (25), obtained from a 10-station representation of the wing are compared in table II with values from the closed-form solution and are seen to be in very good agreement, which indicates that 10 stations are adequate. It is noted that the force distribution, and consequently the divergence parameter, determined by low-aspect-ratio theory is independent of Mach number.

One further check on the accuracy of the iterative solutions based on partitioning the wing into discrete segments was carried out by assuming a polynomial expression for the displacement that satisfied the end conditions and by applying the method of Stodola and Vianello (sec. 5.5, ref. 13) to the loading equation (18). The strip-theory

representation of the aerodynamics was used. With this representation of the loading, another convenient divergence constant K_2 can be defined as

$$K_2 = \frac{q}{\beta E\left(\frac{t_0}{c_0}\right)^3} \tag{48}$$

Iteration on the loading equation with the polynomial expression for the displacement led to a value of K_2 of 60.594. Iteration on the slope equation for the 10-segment, partitioned wing gave a value of K_2 of 60.241.

Solutions Based on Strip Theory

The forces on the various wing segments given by strip theory, equation (9), may be written for use in the slope-influence-coefficient equation (34) as

$$\left\{F_j\right\} = -\frac{8}{\beta}\Delta x q \tan\epsilon\left[x_j\right]\left\{\left(\frac{dh}{dx}\right)_{x_j}\right\}$$

the substitution of which in equation (34) yields

$$\left\{\left(\frac{dh}{dx}\right)_{x_i}\right\} = -\frac{8}{\beta}\Delta x q \tan\epsilon\left[B_{ij}\right]\left[x_j\right]\left\{\left(\frac{dh}{dx}\right)_{x_j}\right\} \tag{49}$$

Alternatively, equation (32) may be used to express the forces in terms of curvature as

$$\left\{F_j\right\} = -\frac{8}{\beta}\Delta x q \tan\epsilon\left[x_j\right]\left[I_1\right]\left\{\left(\frac{d^2h}{dx^2}\right)_{x_j}\right\}$$

so that equation (31) becomes

$$\left\{\left(\frac{d^2h}{dx^2}\right)_{x_j}\right\} = -\frac{8}{\beta}\Delta x q \tan\epsilon\left[A_{ij}\right]\left[x_j\right]\left[I_1\right]\left\{\left(\frac{d^2h}{dx^2}\right)_{x_j}\right\} \tag{50}$$

Either equation (49) or equation (50) may be iterated to convergence to obtain the critical value of q. Results obtained for the flat-plate delta wings of the present study are given in a subsequent section.

Solutions Based on Lifting-Surface Theory

The aerodynamic forces given by lifting-surface theory have been used to develop an iterative solution of the equilibrium equation based on slope influence coefficients. It could be readily modified for use with curvature influence coefficients.

It is recalled that the pressure distribution over the wing is given by a series expression with arbitrary weighting factors a_{nm} which are defined by equation (5) for any specified slope distribution. In concept, one uses equations (5) and (7) to obtain the forces F_j as

$$\left\{F_j\right\} = 8\pi q \left[II_{nm}^{(j)}\right] \left\{a_{nm}\right\} \tag{51a}$$

or

$$\left\{F_j\right\} = 8\pi q \left[II_{nm}^{(j)}\right] \left[II_{LK}\right]^{-1} \left\{\frac{dh}{dx}\right\} \tag{51b}$$

and substitutes this result into equation (34). This provides a form of the equilibrium equation upon which iteration to convergence can be performed.

In practice, it is usually necessary to employ several steps in each cycle of iteration. This is brought about by the fact that the inverse matrix in equation (5) is developed for a particular array of control points which do not, in general, coincide with the midpoints of the segments used in the iterative procedure. To perform one cycle of iteration the following procedure is used: first, assume a set of slopes at the control points and use these slopes in equation (5) to obtain a set of weighting factors a_{nm}; next, use these weighting factors in equation (51a) to obtain the forces F_j; and, finally, substitute the values of the forces into equation (34) to obtain the slopes at the midpoints of the segments. To begin the next cycle of iteration, slopes appropriate to the control-point locations are sorted out of the results of equation (34) and are used in equation (5), and so forth. Usually, convergence is obtained after about four or five cycles of iteration.

DIVERGENCE EFFICIENCY OF A CANTILEVER DELTA WING

As a matter of interest it is noted that one can determine the thickness distribution of the family of distributions expressed by equation (12) for a solid cantilever delta wing that will produce the highest dynamic pressure at divergence for a given total weight.

The weight W of a solid delta wing is found by integrating the thickness distribution and combining the result thus found for the volume with the density $\bar{\rho}$ of the material to give an expression of the form

$$W = k_1 \bar{\rho} t_0 c_0^2 \tan \epsilon \qquad (52)$$

where the form of the constant k_1 depends on the form of the thickness distribution. This result may be used together with the closed-form result for the divergence parameter given by equation (25) to obtain the expression

$$\frac{q_d}{W^3} = \frac{K_1}{k_1^3} \frac{EK_0}{\bar{\rho}^3 c_0^9 \tan^4 \epsilon}$$

Expressions of the same general form are obtained from the iterative solutions and from the various aerodynamic theories.

Values of q_d/W^3 obtained with low-aspect-ratio theory and with piston theory are shown in figure 3 for the thickness distribution given by equation (12) for $m = 0$. The values of q_d/W^3 have been normalized to the value for the constant-thickness wing ($n = 0$). The thickness distribution for maximum mass efficiency could be determined by variational procedures; however, the maximum value of q_d/W^3 and the associated thickness distribution would not differ appreciably from the results for $n = 1$.

APPARATUS AND TESTS

Models

A series of delta-wing models of constant thickness and of apex half-angles of 5°, 10°, 15°, and 20° were constructed. A sketch of the various model configurations is presented in figure 4. The thickness

at the base of the delta wing before attachment to the wind-tunnel sting was increased to simulate cantilever base boundary conditions with a minimum of aerodynamic interference. For the transonic tests, two model configurations were used. Both configurations had a 10-inch chord with one model constructed of 0.048-inch-thick aluminum alloy and the other of 0.0385-inch-thick aluminum alloy. For the supersonic and hypersonic tests, wings of 0.048-inch-thick aluminum alloy with a 6-inch chord were used.

Wind-Tunnel Tests

Transonic tests.- Divergence data were obtained at transonic speeds with the models mounted on a sting in the Langley 2-foot transonic aeroelasticity tunnel with Freon-12 as a test medium. The tunnel Mach number was held constant and the test-section density, and hence dynamic pressure, was slowly increased until divergence occurred. Occasional adjustments in the sting angle of attack were required to correct for changes in tunnel-flow angularity so that the model would remain at zero lift until the divergence dynamic pressure was reached. Small, relatively high-frequency oscillations of predominantly the apex region of the delta wing usually occurred at low dynamic pressure and continued intermittently as the dynamic pressure was increased up to the divergence condition. These oscillations were believed to be associated with flow separation or with flow irregularities in the tunnel stream and with low structural damping of the models. The divergence dynamic pressures were very sharply defined and were marked by one or two large excursions of the tip of the model just prior to divergence. The high-frequency oscillations of the tip region usually continued intermittently during the preliminary excursions and during the divergence. It was not determined whether these oscillations had any effect on the divergence characteristics of the models; however, the data faired fairly well with the supersonic data where the oscillations were not apparent. The model motion, when divergence was reached, was very rapid, with the deflection increasing until the model was bent past 90° to the airflow. Some of the models after testing are shown in figure 5.

Supersonic and hypersonic tests.- The supersonic tests at $M = 2.0$ and $M = 3.0$ were conducted in the Langley 9- by 18-inch supersonic aeroelasticity tunnel with air used as a test medium. The hypersonic tests at $M = 7.3$ were made in the Langley hypersonic aeroelasticity tunnel which uses helium as a test medium. The test procedures at supersonic and hypersonic speeds were the same. The models were mounted on a sting and the tests were made at a fixed Mach number. The stagnation pressure was increased until the model diverged. A strain gage on each model was used to correlate the time of divergence with the recorded tunnel dynamic pressure. Each complete test lasted from 4 to 10 seconds. There was insufficient time to adjust the model angle of

attack during a test and several models that were not alined properly slowly loaded up and failed. They were discarded and the tests were remade with new models.

RESULTS AND DISCUSSION

The transonic and hypersonic divergence data of the present investigation are presented in figures 6 and 7. Experimental results are compared with results of calculations based on small-aspect-ratio theory, lifting-surface theory, and strip theory. A nondimensional divergence parameter $\frac{q_d}{E\left(\frac{t_0}{c_0}\right)^3}$, in which q_d denotes the dynamic pressure at divergence, is employed in presenting the results. In figures 6(a) to 6(e), the divergence parameter is plotted as a function of the apex half-angle for the different Mach numbers. In figure 7, the divergence parameter is plotted as a function of Mach number for the four different apex half-angles used. In figures 6 and 7 the solid portions of the curves indicate the range of Mach numbers or apex half-angles for which the theories might be expected to be valid. Thus, for small-aspect-ratio theory the solid curves denote conditions where the Mach angle is at least twice the apex half-angle, and for strip theory the solid lines denote conditions where the component of stream velocity normal to the leading edge is supersonic.

Examination of the experimentally determined values of the divergence parameter shows that for a given Mach number (figs. 6(a) to 6(e)) q_d increases with decreasing apex angle and for a given apex angle (fig. 7) q_d increases with increasing Mach number. With regard to the various analytical approaches to be considered, the figures illustrate the following facts: Small-aspect-ratio theory is independent of Mach number and inversely proportional to $\tan \epsilon$; strip theory is independent of apex angle and directly proportional to β; and lifting-surface theory is a function of both Mach number and apex angle.

At $M = 0.8$ (fig. 6(a)) lifting-surface theory and small-aspect-ratio theory give very similar results. For $\epsilon = 20^\circ$, both indicate values of q_d well above that found experimentally and become increasingly high relative to experiment as ϵ decreases. Several approaches were taken in trying to improve the results given by subsonic lifting-surface theory. In obtaining the aerodynamic forces three different arrays of control points were used, including one distribution based on Gaussian techniques. In performing the iterations on the equilibrium

equation the 16-segment system shown in figure 2, with close spacing near the leading edge, was used to examine the possibility that the chordwise centers of pressure might be too far removed from the centers of the forward segments in the 10-segment system. The results were essentially insensitive to these changes.

For the ranges of Mach number and apex angle for which small-aspect-ratio theory might be expected to apply in supersonic flow, values of dynamic pressure at divergence predicted by this theory are generally above the experimentally determined values. When applied beyond the range of expected validity, small-aspect-ratio theory predicts values of q_d well below experiment.

For Mach numbers above about 2.0 lifting-surface theory (and strip theory for supersonic leading edges) predicts the experimental trends quite well except for the wing having an apex half-angle of 5°. For this case none of the theoretical approaches used gives adequate agreement, possibly because viscous effects may be quite strong. When strip theory is applied for subsonic leading edges, the predicted values of divergence dynamic pressure are generally quite conservative; first-order piston theory would yield values higher by the factor M/β.

CONCLUSIONS

The results of the analysis of the static divergence of low-aspect-ratio triangular wings and the comparisons of these theoretical results with the experimental data lead to the following conclusions:

1. A general iteration procedure is developed for computing divergence dynamic pressures for delta wings using aerodynamic forces given by small-aspect-ratio theory, lifting-surface theory, and strip theory. The procedure can be extended to arbitrary planforms and other aerodynamic representations.

2. Certain special thickness distributions led to closed-form solutions for the divergence dynamic pressure when the aerodynamic forces were given by small-aspect-ratio theory. The closed-form solutions were useful for evaluating the numerical procedures.

3. At a given Mach number the experimental divergence dynamic pressures of the cantilever delta models of uniform thickness, which were tested, increased with decreasing apex angle; for a given apex angle the experimental divergence dynamic pressures increased with increasing Mach number.

4. In subsonic flow lifting-surface theory and small-aspect-ratio theory give very similar results but predict dynamic pressures at divergence which are high relative to experiment.

5. Values of dynamic pressure at divergence given by small-aspect-ratio theory vary from generally above experiment in the ranges of Mach number and apex angle for which the theory is expected to be valid to well below experiment for conditions outside this range.

6. For Mach numbers above about 2.0 lifting-surface theory (and strip theory for supersonic leading edges) predicts the experimental trends quite well except for the wing with an apex half-angle of 5° for which viscous effects may be important.

Langley Research Center,
National Aeronautics and Space Administration,
Langley Field, Va., June 9, 1960.

REFERENCES

1. Biot, M. A.: Aero-Elastic Stability of Supersonic Wings. Chordwise Divergence - The Two-Dimensional Case. Rep. No. 1, Cornell Aero. Lab., Dec. 8, 1947.

2. Biot, M. A.: The Divergence of Supersonic Wings Including Chordwise Bending. Jour. Aero. Sci., vol. 23, no. 3, Mar. 1956, pp. 237-251.

3. Miles, John W.: Chordwise Divergence of Delta Wings. Rep. No. AL-1197, North American Aviation, Inc., Nov. 21, 1950.

4. Hedgepeth, John M., and Waner, Paul G., Jr.: Analysis of Static Aero-elastic Behavior of Low-Aspect-Ratio Rectangular Wings. NACA TN 3958, 1957.

5. Martin, Dennis J., and Watkins, Charles E.: Transonic and Supersonic Divergence Characteristics of Low-Aspect-Ratio Wings and Controls. Rep. No. 59-58, Inst. Aero. Sci., Jan. 1959.

6. Rainey, A. Gerald, Hanson, Perry W., and Martin, Dennis J.: Experimental and Analytical Investigation of Transonic and Supersonic Divergence Characteristics of a Delta-Plan-Form Model of the Canard Control Surface of an Air-To-Ground Missile. NACA RM L58E07, 1958.

7. Jones, Robert T.: Properties of Low-Aspect-Ratio Pointed Wings at Speeds Below and Above the Speed of Sound. NACA Rep. 835, 1946. (Supersedes NACA TN 1032.)

8. Garrick, I. E.: Some Research on High-Speed Flutter. Third Anglo-American Aero. Conf., Sept. 4-7, 1951 (Brighton, England). R.A.S., 1952, pp. 419-446J.

9. Watkins, Charles E., Woolston, Donald S., and Cunningham, Herbert J.: A Systematic Kernel Function Procedure for Determining Aerodynamic Forces on Oscillating or Steady Finite Wings at Subsonic Speeds. NASA TR R-48, 1959.

10. Miles, John W.: On Simple Plan Forms in Supersonic Flow. Jour. Aero. Sci. (Readers' Forum), vol. 17, no. 2, Feb. 1950, p. 127.

11. Miles, John W.: On Harmonic Motion of Wide Delta Airfoils at Supersonic Speeds. NAVORD Rep. 1234 (NOTS 294), U.S. Naval Ord. Test Station (Inyokern, Calif.), June 13, 1950.

12. Ashley, Holt, and Zartarian, Garabed: Piston Theory - A New Aerodynamic Tool for the Aeroelastician. Jour. Aero. Sci., vol. 23, no. 12, Dec. 1956, pp. 1109-1118.

13. Hildebrand, F. B.: Advanced Calculus for Engineers. Prentice-Hall, Inc., 1949.

TABLE I.- SECTION MOMENT-OF-INERTIA CONSTANT K_0 FOR VARIOUS SPANWISE SECTIONS

$$\left[I(x) = \frac{1}{6} \int_0^{x \tan \epsilon} t^3(x,y)dy = K_0 \frac{t_0^3}{6} \left(\frac{x}{c_0}\right)^n x \tan \epsilon \right.$$

$$\left. \text{when } t(x,y) = t_0 \left(\frac{x}{c_0}\right)^{n/3} \left(1 - \frac{y^2}{s^2}\right)^{m/12} \right]$$

m	K_0
0	1.0000
1	.8740
2	.7854
4	.6667
6	.5891
12	.4571

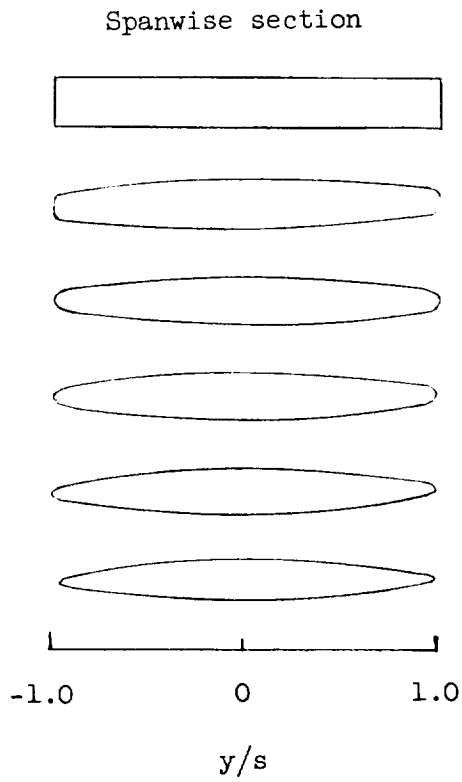

TABLE II.- COMPARISON OF RESULTS OF EXACT AND ITERATIVE SOLUTIONS FOR VARIOUS CHORDWISE SECTIONS AND CONSTANT SPANWISE SECTION

$$\left[t(x,y) = t_0\left(\frac{x}{c_0}\right)^{n/3}\right]$$

n	$K_1 = \frac{q_d \tan \epsilon}{EK_0\left(\frac{t_0}{c_0}\right)^3}$		
	Exact solution	Iteration on curvature equation (31)	Iteration on slope equation (34)
0	49.5	49.2	49.4
1	37.7	37.3	37.3
2	25.08	24.49	24.48
3	8.58	8.54	8.42

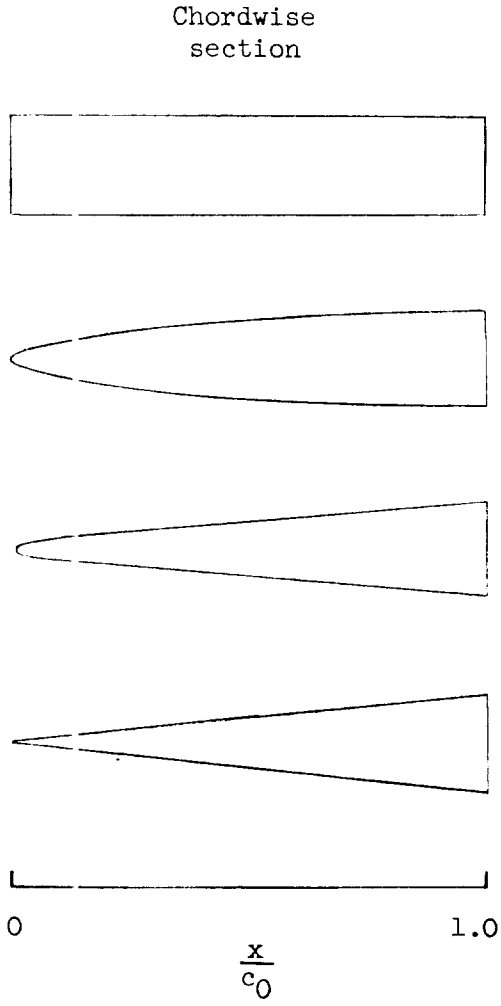

TABLE III.- INTEGRATING MATRIX $\left[I_1\right]$ FOR EQUATION (32)

$\left[\text{Common factor, } \frac{c_0}{10}\right]$

0.2541	1.9126	-1.3974	6.0090	-6.6564	9.4773	-5.7545	4.8079	-0.4640	1.3115
-0.0329	0.6105	0.1557	3.8041	-4.2750	7.6157	-4.7357	4.4375	-0.3837	1.3036
-0.0250	0.2446	-0.7912	4.4101	-4.8225	8.0083	-4.9398	4.5092	-0.3988	1.3051
-0.0265	0.2671	-1.2230	3.6389	-4.5240	7.8297	-4.8547	4.4808	-0.3930	1.3046
-0.0259	0.2602	-1.1758	3.1415	-5.1803	7.9904	-4.9184	4.5003	-0.3968	1.3049
-0.0263	0.2642	-1.1982	3.2299	-5.7500	7.4208	-4.8299	4.4779	-0.3928	1.3046
-0.0259	0.2604	-1.1788	3.1662	-5.5893	6.7644	-5.3273	4.5250	-0.3998	1.3051
-0.0265	0.2662	-1.2072	3.2513	-5.7678	7.0629	-6.0985	4.0932	-0.3772	1.3036
-0.0250	0.2510	-1.1355	3.0472	-5.3753	6.5154	-5.4926	3.1463	-0.7431	1.3115
-0.0329	0.3314	-1.5058	4.0660	-7.2368	8.8969	-7.6975	4.6994	-2.0452	1.0246

TABLE IV.- DIFFERENTIATING MATRIX $[D]$ FOR EQUATION (44)

$$\left[\text{Common factor, } \frac{1}{12\Delta x}\right]$$

$$\begin{bmatrix}
-25 & 48 & -36 & 16 & -3 & 0 & 0 & 0 & 0 & 0 \\
-3 & -10 & 18 & -6 & 1 & 0 & 0 & 0 & 0 & 0 \\
1 & -8 & 0 & 8 & -1 & 0 & 0 & 0 & 0 & 0 \\
0 & 1 & -8 & 0 & 8 & -1 & 0 & 0 & 0 & 0 \\
0 & 0 & 1 & -8 & 0 & 8 & -1 & 0 & 0 & 0 \\
0 & 0 & 0 & 1 & -8 & 0 & 8 & -1 & 0 & 0 \\
0 & 0 & 0 & 0 & 1 & -8 & 0 & 8 & -1 & 0 \\
0 & 0 & 0 & 0 & 0 & 1 & -8 & 0 & 8 & -1 \\
0 & 0 & 0 & 0 & 0 & -1 & 6 & -18 & 10 & 3 \\
0 & 0 & 0 & 0 & 0 & 3 & -16 & 36 & -48 & 25
\end{bmatrix}$$

L-582

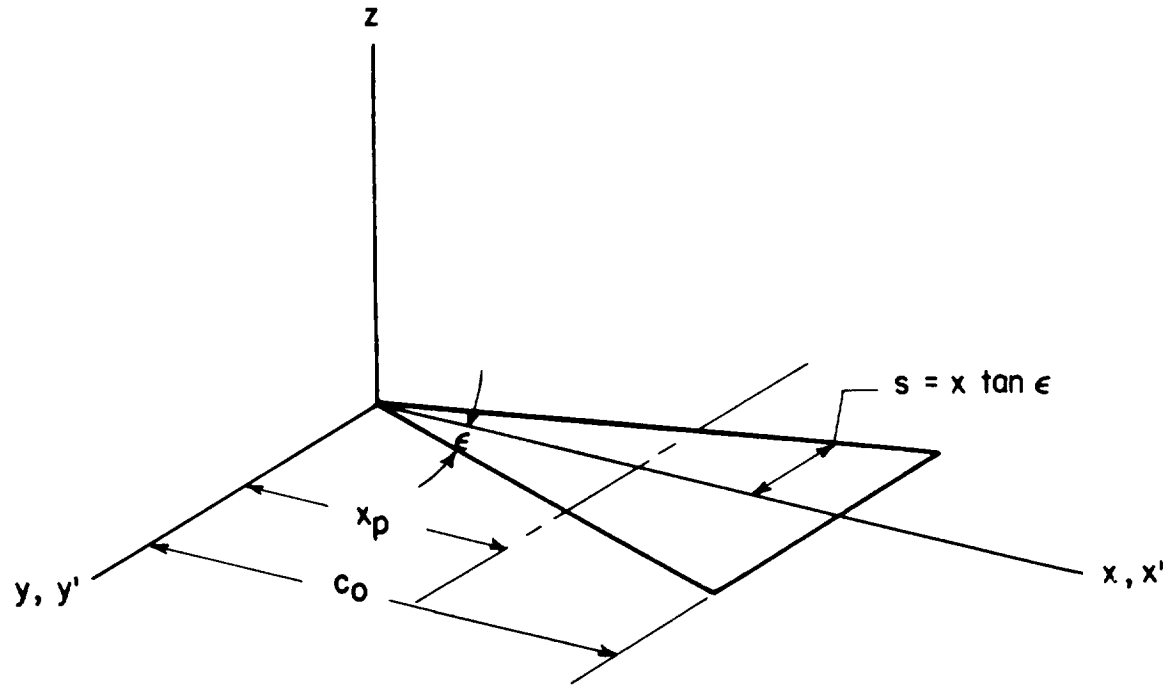

Figure 1.- Coordinate system.

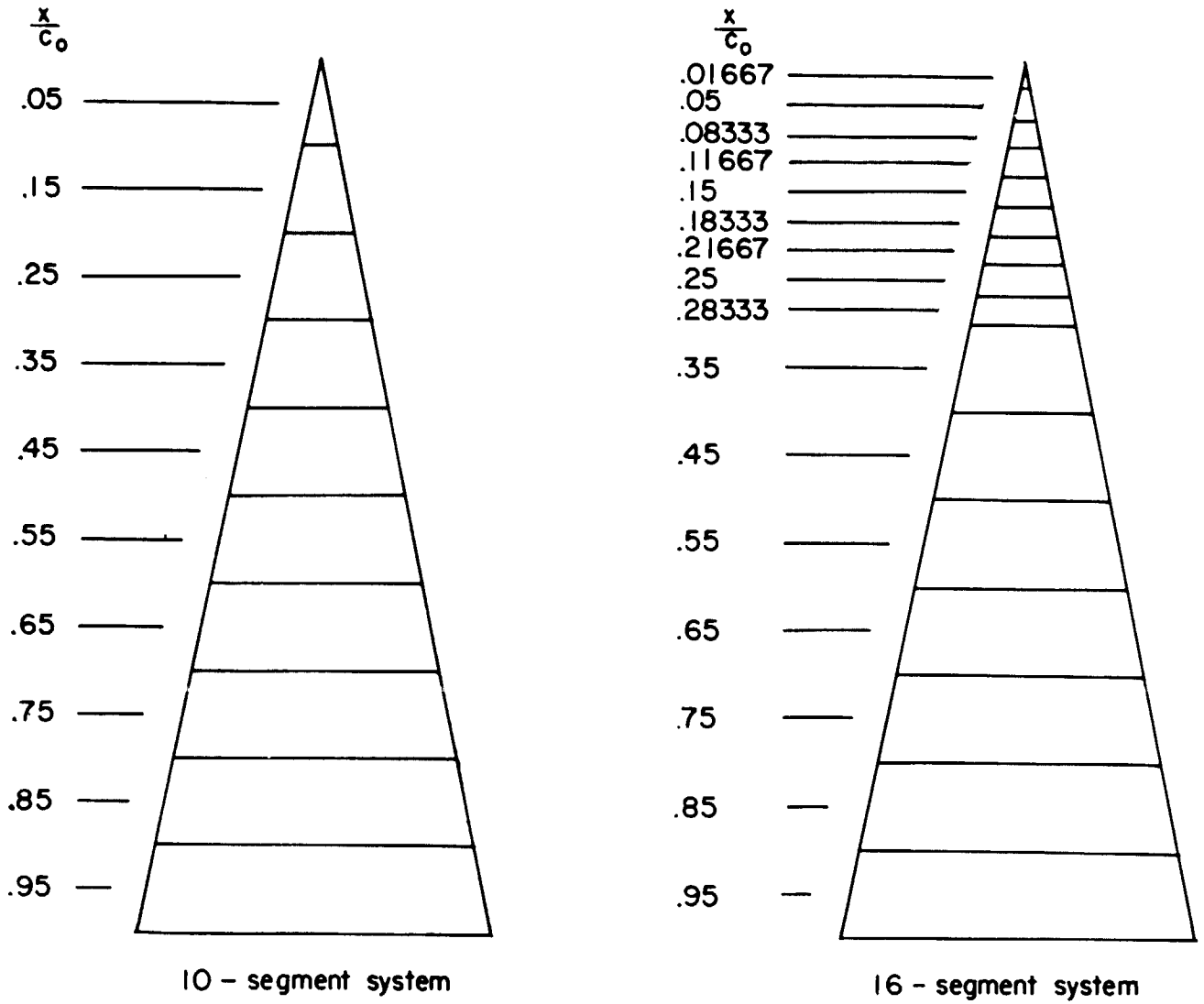

Figure 2.- Sketches showing wing segments for iterative solutions.

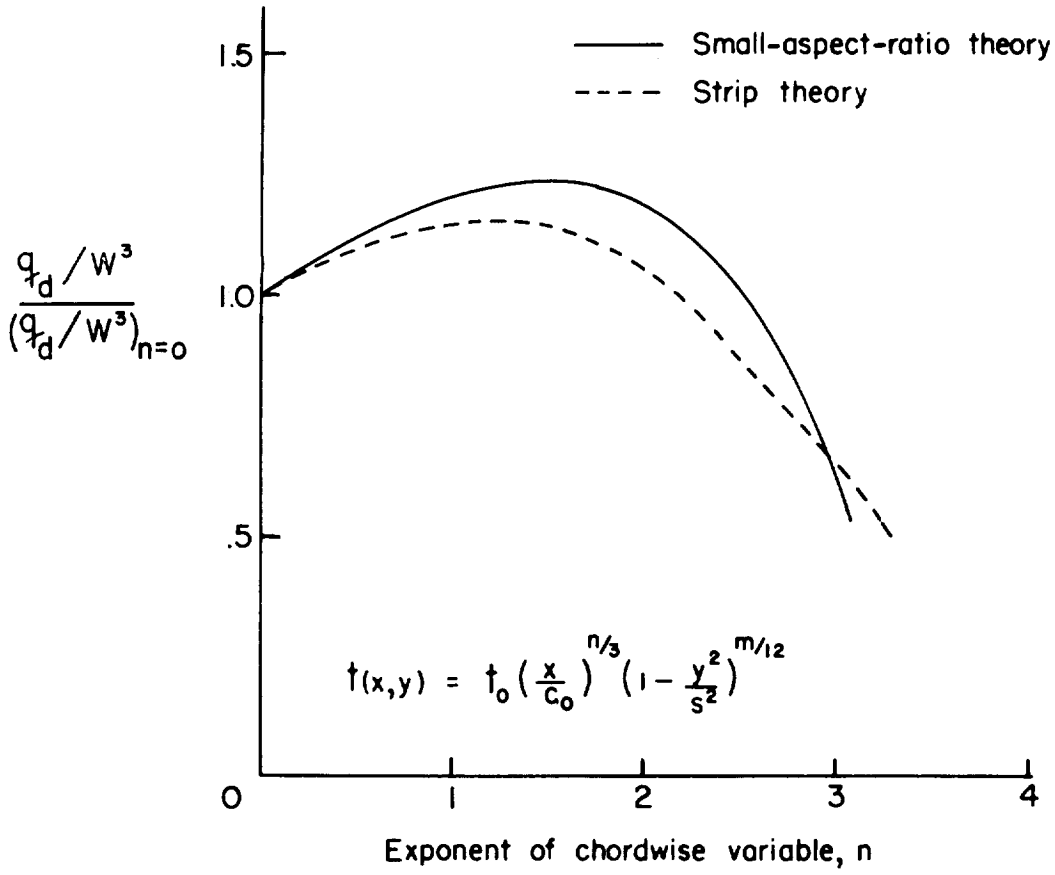

Figure 3.- Divergence efficiency factor.

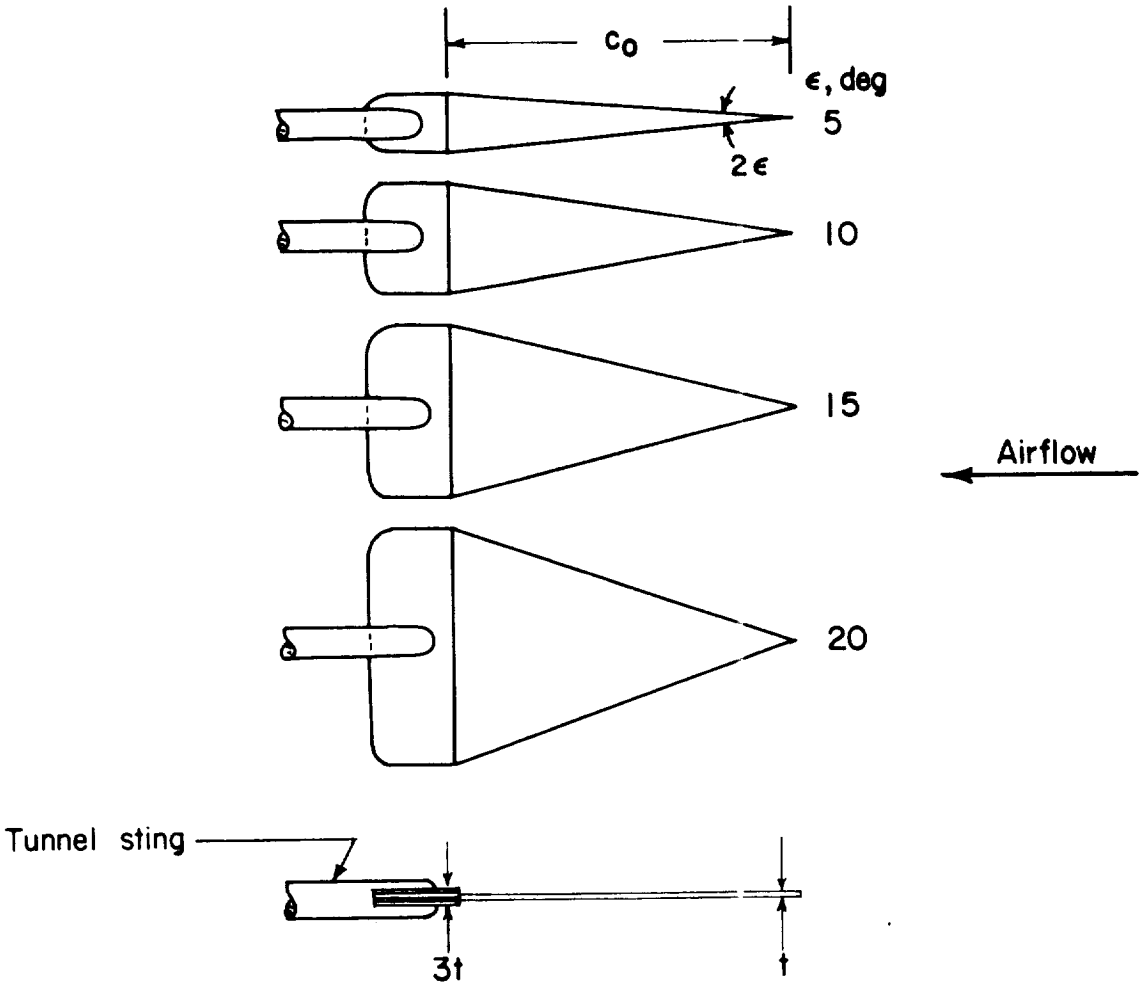

Figure 4.- Sketch of divergence models on sting.

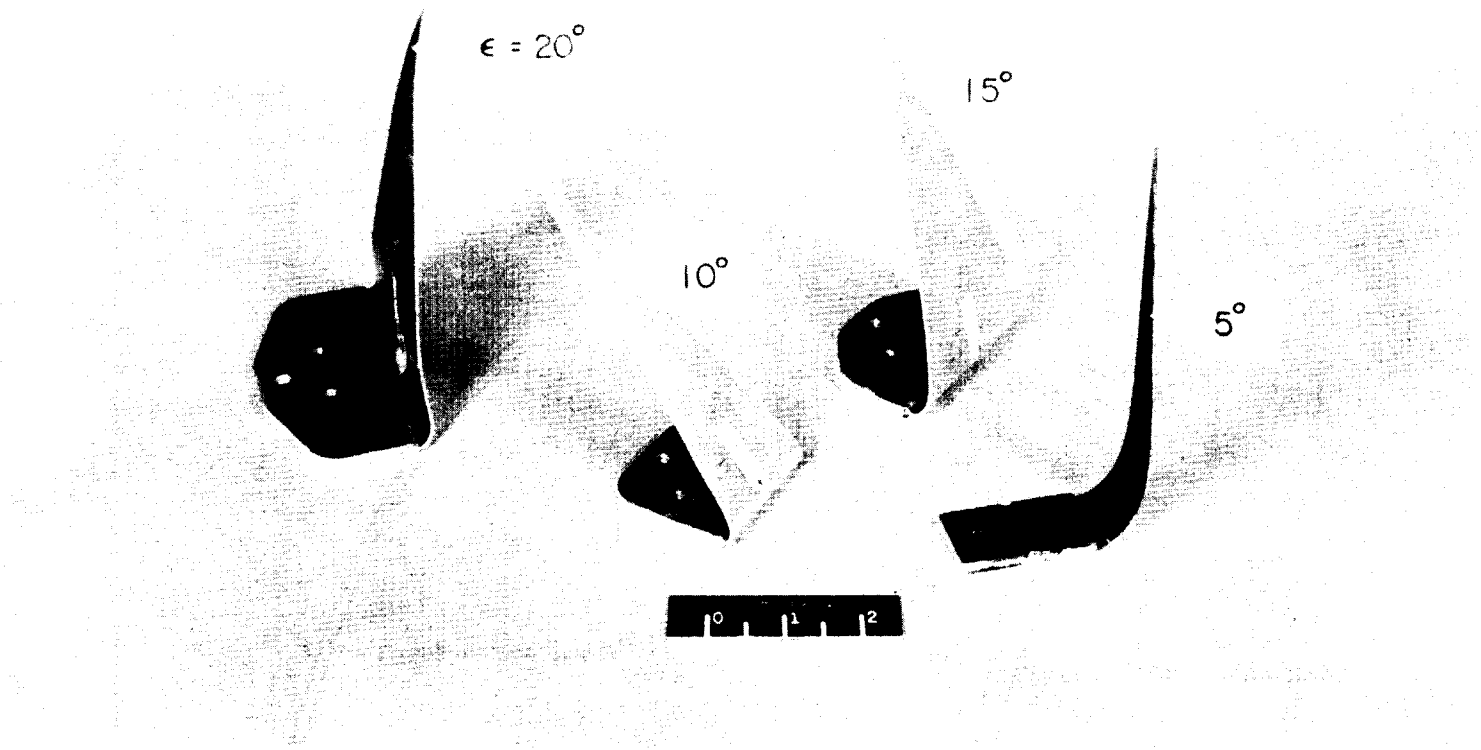

Figure 5.- Typical models after divergence. L-59-7665.1

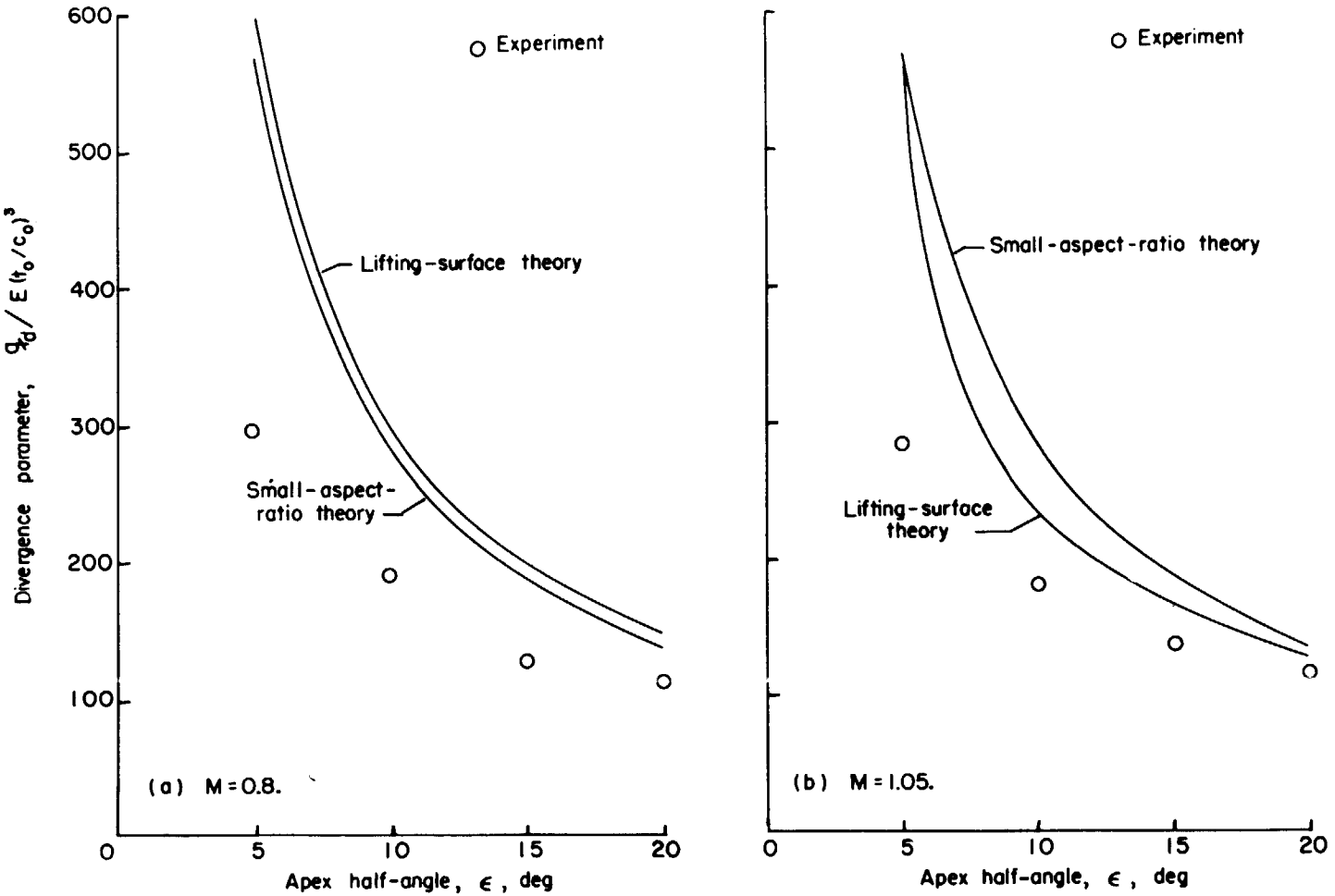

Figure 6.- Comparison of theoretical and experimental values of the divergence parameter $q_d/E(t_0/c_0)^3$ for various values of apex half-angle ϵ.

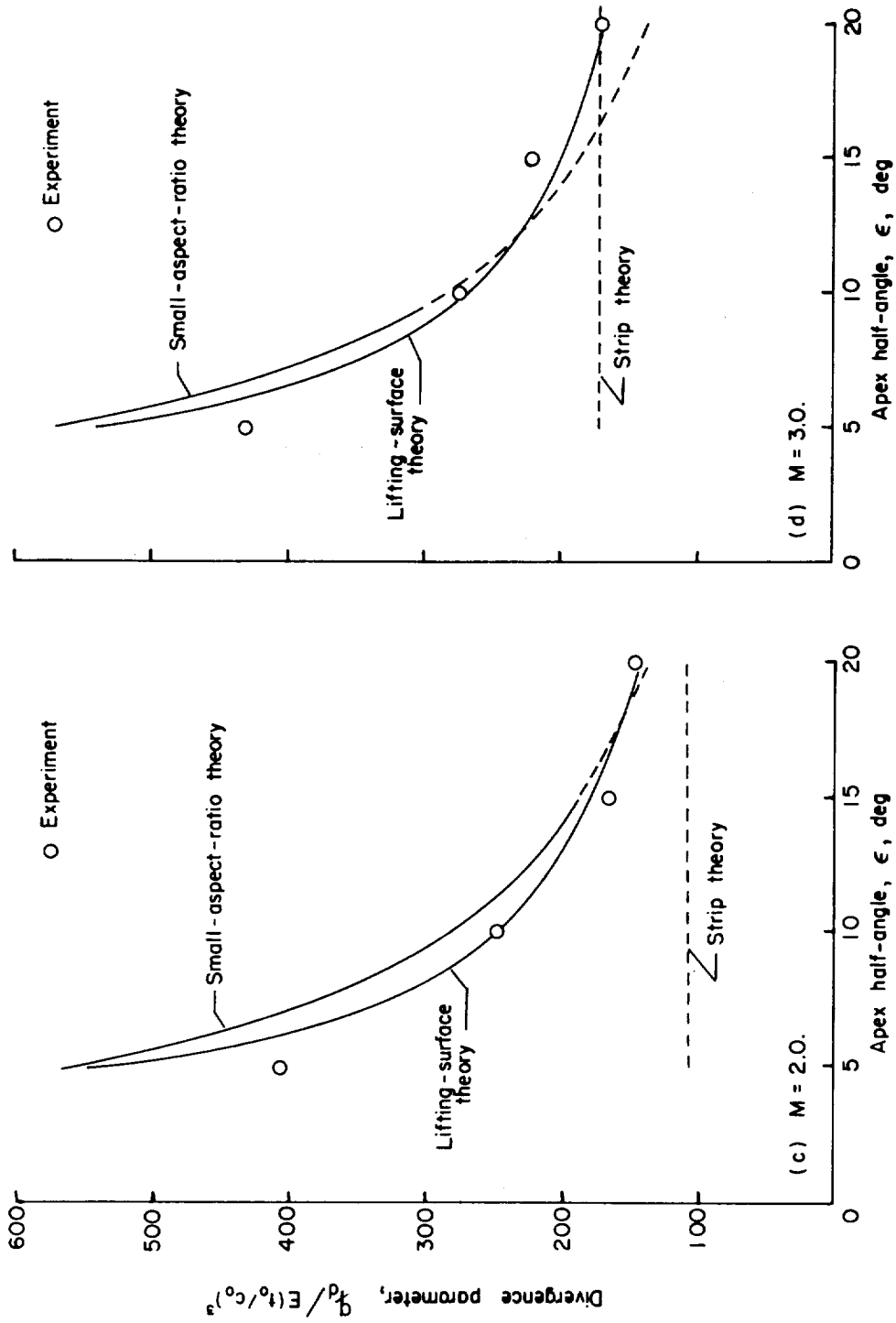

Figure 6.- Continued.

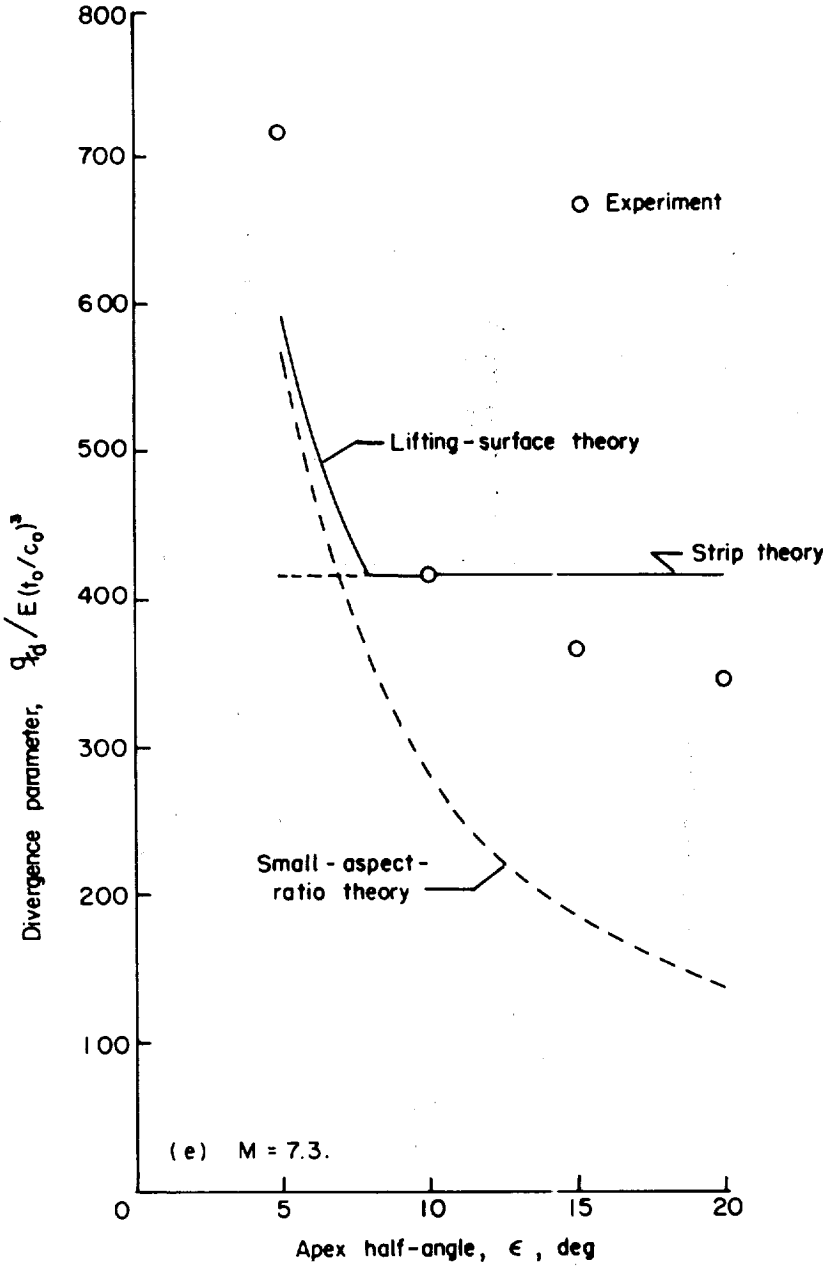

Figure 6.- Concluded.

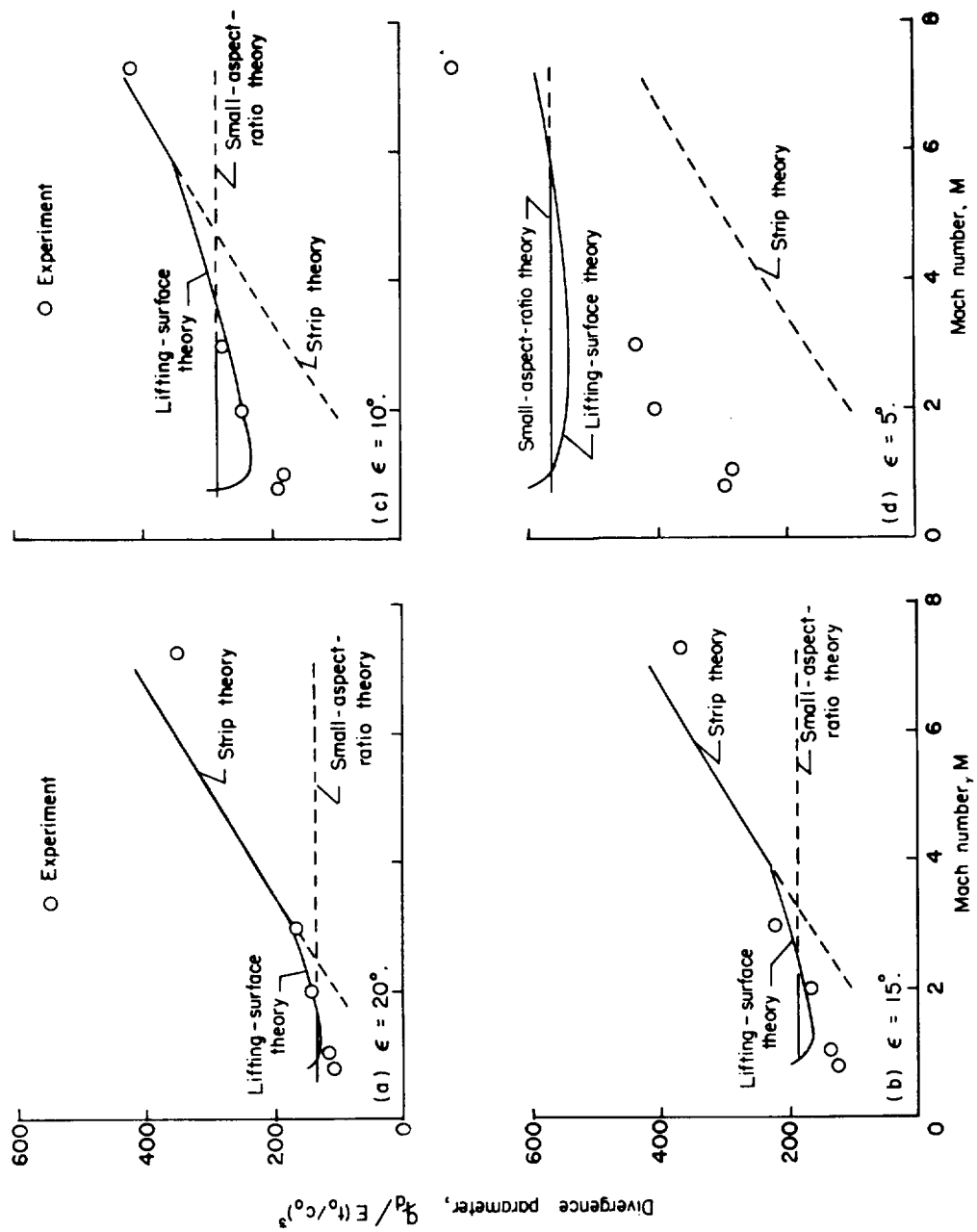

Figure 7.- Variation of divergence parameter $q_d/E(t_o/c_o)^3$ with Mach number.